Theor Chem Acc (2012) 131:1174
DOI 10.1007/s00214-012-1174-2

REGULAR ARTICLE

Density functional study of substituted (–SH, –S, –OH, –Cl) hydrated ions of Hg^{2+}

Akef T. Afaneh · Georg Schreckenbach · Feiyue Wang

Received: 12 January 2012 / Accepted: 17 January 2012 / Published online: 17 March 2012

Abstract The electronic structure of Hg(II) ions, $[Hg(L)_n(H_2O)_m]^q$ ($L = HO^-$, Cl^-, HS^-, S^{2-}) has been studied. Geometries were fully optimized. The B3LYP and PBE functionals give structures in good agreement with available experimental data. Calculated stretching frequencies generally correlate well with bond lengths. The role of the water molecule(s) in the solvated Hg(II) complexes has been investigated. The solvent can act as nucleophile, as hydrogen bond acceptor or as a spectator. The trans-effect results in lengthening of the Hg–L bond length. It can be understood as a competition between ligands in trans positions for the ability to donate their electron density to the 6s AO of Hg(II). The effect of the presence of water molecules on the Hg–L bond length depends on whether or not the water molecules form a direct coordination bond with Hg(II); it will not guarantee an increase in the stability of the complexes. The interaction energy, which represents the interaction between Hg(II) and ligand L and excludes all other interactions, is nucleophilicity-dependent. The interaction energy and the strength of the ligand nucleophilicity follow the order: $S^{2-} > HS^- > HO^- > Cl^- > H_2O$. The charge transfer, ΔN, is an indication for the type and strength of the interaction between ligand and Hg(II). Increasing the positive and negative value of ΔN will decrease and increase the Hg(II) total NBO charge, respectively, while decreasing the electrophilicity of Hg(II) will decrease its charge and the charge transfer, ΔN.

Keywords Density functional theory · Mercury (II) complexes · Microsolvation · Hard soft acid base principle (HSAB) · Natural bond orbital analysis (NBO)

1 Introduction

Mercury (Hg) is an environmental contaminant with elevated concentrations frequently observed in the atmosphere [1, 2], natural waters [3, 4] and the human body [5]. In the atmosphere, elemental Hg and small molecule halides and oxides are thought to be the most important species, while in aqueous solution, sulfidic, halides and hydroxidic species are often important. Within biota including humans, organometallic Hg compounds and species with Hg–S bonds are the most dominant [5]. Thus, environmentally important reactions of Hg involve Hg hydroxides, sulfides, bisulfides (sulfhydryls, –SH) and halides. The low reactivity of gaseous elemental Hg(0) (GEM) in the atmosphere is primarily responsible for its long-range transport around the globe. However, several recent studies indicate that GEM is rapidly photooxidized to Hg(II) compounds known as reactive gaseous mercury (RGM) in the Arctic region during polar sunrise [6–8].

In solution, the Hg(II) ion tends to be surrounded by octahedrally arranged water molecules to give, in effect, $[Hg(H_2O)_6]^{2+}$. This arrangement is disturbed if one or more of the water molecules dissociate or if deprotonation of one or more of the water molecules occurs. In either

Electronic supplementary material The online version of this article (doi:10.1007/s00214-012-1174-2) contains supplementary material, which is available to authorized users.

A. T. Afaneh · G. Schreckenbach (✉) · F. Wang
Department of Chemistry, University of Manitoba, Winnipeg, MB R3T 2N2, Canada
e-mail: schrecke@cc.umanitoba.ca

F. Wang
Centre of Earth Observation Science, Department of Environment and Geography, University of Manitoba, Winnipeg, MB R3T 2N2, Canada

case, this results in $[Hg(L)_n(H_2O)_m]^q$, more briefly written as $[HgL_n]^q$.

The explanations of factors determining the specificity of metal ion uptake are often based on qualitative or semi-quantitative theories or principles, such as the HSAB (hard and soft acids and bases) principle of Parr and Pearson [9, 10], the Irving–Williams series of stability constants [11, 12] or the empirically observed abundance of specific geometries for a given transition metal (TM) in a given oxidation state [13, 14]. Besides, there have been attempts to model TM complexes by molecular mechanics [15, 16] and the achievements have been reviewed by Comba [17]. However, it should be stressed that TM systems are challenging even for the sophisticated quantum chemical theories, which implies that one cannot necessarily expect to obtain an accurate description of their properties and structures with the force field (molecular mechanics) approach.

High-level quantum chemical methods can be applied to the quantitative and accurate modeling of TM complexes. In the past decade, a huge amount of papers dealing with theoretical calculations of various TM systems have been published, and we refer the reader to some recent and older reviews [4, 5, 18–28]. In the next paragraph, we confine ourselves to the theoretical studies pertinent to this work.

An understanding of mercury bonding or interaction is essential to understand and anticipate possible reactions, bioavailability and toxicity of mercury in the environment. Several authors [29–44] have treated the interaction between the bare mercury ion and small molecule(s) or ions theoretically. Wienderhold et al. [45], Schauble [46], Filatov and Cremer [29], Cremer et al. [30] and Peterson et al. [31–39] performed theoretical calculations at different levels of theory on the stability of Hg-chalcogenides and Hg-halogens. Cremer et al. [29, 30] showed that the Hg–S bond is weaker than the Hg–OH, Hg–SH and Hg–Cl bonds. These findings are in contradiction with the HSAB principle. The quantum chemical studies of mercury complexes that are perhaps most relevant to the current work are those of the Peterson group [31–39] and those by Tossell [40–44]. Each of these investigations focused on selected mercury compounds $[HgL_n]^q$ ($L = Cl^-$, HO^-, HS^- and S^{2-}). However, the latter author did not attempt to perform a comprehensive study of mercury bonding by varying the number of H_2O molecules, while the former authors, Peterson et al. [32], did this with one, two and three water molecules. Therefore, it is important to study the interaction of other mercury species with larger explicit solvation spheres, which has not previously appeared in the literature.

The aim of the current work is to provide a thorough and comparative study of the interactions of the Hg(II) ion with different functional groups (attached to it in defined coordination modes), specifically water, H_2O; hydroxide, OH^-; sulfide, S^{2-}; bisulfide, HS^-; and chloride, Cl^-. The effects of finite numbers of first- and second-coordination-sphere waters (microsolvation) are investigated. Furthermore, we attempt to evaluate precisely the small differences in interaction energies of Hg(II) ion with different ligands and to investigate the factors determining their affinity and selectivity toward Hg^{2+}. Moreover, we study the properties of the Hg(II) ion and the ligands, Cl^-, OH^-, HS^- and S^{2-}, that characterize their ability to act as an acid or base, that is, the ability to donate or accept electronic charge (HSAB principle). To achieve this, we compute electronegativity, χ; chemical hardness, η; chemical potential, μ; and the global electrophilicity, ω^+ for a series of Hg(II) complexes. We also compute the charge transfer, ΔN, for bringing these ligands and $[Hg(H_2O)_m]^{2+}$ together.

1.1 Computational details

Geometry optimizations for the gas-phase Hg(II)–ligand complexes were carried out with two different density functionals and a variety of basis sets. In order to confirm that the resulting geometries correspond to minima on the potential energy surface, vibrational frequencies were computed as well. All the calculations were performed in the framework of density functional theory (DFT). Unless otherwise noted, the calculations were carried out using the Gaussian03 program (B05 version) [47]. The three-parameter functional developed by Becke [48], which combines Becke's gradient-corrected exchange functional and the Lee–Yang–Parr and Vosko–Wilk–Nusair correlation functionals [49–51] with part of the exact Hartree–Fock exchange energy, has been employed (denoted as B3LYP). This is combined with various effective core potentials and basis sets (see below) for geometry optimizations, vibrational analyses and electronic structure calculations of aqueous complexes. For the Hg(II) ion, we used the Stuttgart–Dresden basis set (SDD) [52] with the respective effective core potential to treat the scalar relativistic effects.

Calculations have also been performed with the Amsterdam Density Functional package (ADF 2008 [53]). The zero-order regular approximation (ZORA) [54] to the Dirac equation has been applied to the $[Hg(L)_n(H_2O)_m]^q$ molecules in the variant where spin–orbit interaction was neglected (scalar relativistic approximation). To understand the nature of the Hg–L bond in the Hg(II) complexes, the $[Hg(L)_n(H_2O)_m]^q$ formation energy was decomposed into orbital interaction energy, electrostatic energy, Pauli electron repulsion and strain energy using the energy decomposition scheme of Ziegler and Rauk [55], as implemented in ADF 2008 [53]. Both the geometry optimization and energy decomposition calculations were

performed using the PBE functional [56]. Uncontracted Slater-type orbitals were used as basis functions. The valence basis functions have triple-ζ quality, augmented with two sets of p functions for Hg, Cl and S, but with only one set of p functions for the other atoms, ZORA-TZ2P and ZORA-TZP. The $(1s)^2$ core electrons of O, the $(1s2sp)^{10}$ core electrons of Cl^- and S^{2-}, and the $(1s2sp3spd4spdf)^{60}$ core electrons of Hg(II) were treated within the frozen-core approximation [57].

We determined the structures of the complexes as follows. Thirty water molecules were added to each solute in an approximately spherical shape, using the GaussView graphical interface. We optimized the corresponding structures at the B3LYP (G03) and PBE (ADF 2008) levels of theories using SDD/cc-pVTZ and TZP basis sets, respectively. Next, we removed all the water molecules that formed the third, fourth and higher solvation layers. We repeated these optimization steps with each ligand and followed the same procedure. Finally, we got the structures of the Hg(II) complexes as shown in Figs. 1 and S1–S7 (Supporting Information).

We examined basis set convergence by increasing the size of the basis set for Hg(II) and the ligands. For Gaussian 03, we used 6-311+G(d), 6-311G(dp) 6-311+G(d,p) and cc-pVTZ for the ligands, and SDD with ECP for Hg(II), then increased the basis set for Hg(II) using cc-pVTZ-PP with ECP. For the ADF 2008 code, we used TZP for all the atoms in the complexes using the scalar ZORA method for relativistic effects, and then increased the basis set size only on Hg(II), S and Cl by using TZ2P and TZP for O and H atoms. After that, we calculated the free energies of formation of the corresponding ligands; see Table 4 below and supporting material (Table S8). The data in these two tables indicate that the best level of basis set, which can be considered as converged, is cc-pVTZ//cc-pVTZ-PP. Consequently, we report results at this level only, unless otherwise stated.

In order to analyze the charge distribution and to better understand the intramolecular interactions in the system, the second-order perturbation theory analysis of the Fock matrix in the natural bond orbital (NBO) [58] analysis was performed on the optimized electronic densities using the NBO program as implemented in the Gaussian 03 package. This analysis provides an improvement over the Mulliken population analysis often used in the description of the charge distribution.

1.2 Pearson's principle

Two quantities central to DFT, μ and η [10, 59], measure the response of the electronic energy ($E[\upsilon, N]$) to electron transfer and redistribution, initiated by a chemical reaction. The linear response is μ,

$$\mu = -\chi = \left(\frac{\partial E}{\partial N}\right)_{\upsilon} \cong -\frac{IP + EA}{2} \quad (1)$$

N is the number of electrons, and $\upsilon(r)$ is the external potential. In practice, the approximation of finite

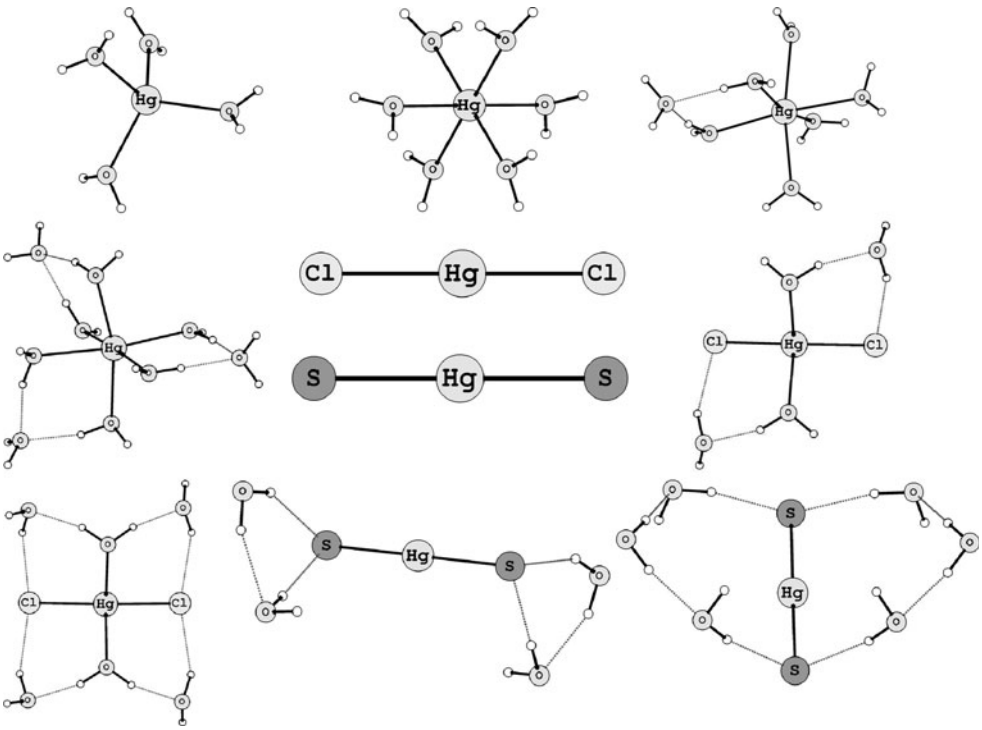

Fig. 1 Selected equilibrium geometries of $[Hg(H_2O)_m]^{2+}$ and $[Hg(L)_n(H_2O)_m]^q$ ($n = 1, 2$; $m = 0, 1, 5, 6, 7, 9$; $q = 2 - n$ for $L = HO^-, Cl^-, HS^-$ and $q = 2 - 2n$ for $L = S^{2-}$) complexes computed at the B3LYP/cc-pVTZ//SDD (ECP) level of theory

differences, the slope of the curve of energy against the number of electrons, maintaining the external potential constant, can be described in terms of the ionization potential, IP, and the electronic affinity, EA. Thus, the chemical potential can be associated with the negative of Mulliken's electronegativity (χ) [60] in the form of Eq. 1. Physically, μ corresponds to the capacity of a system to donate electron density. The electron transfer between reactants flows from high to low μ. The curvature corresponds to the system's hardness:

$$\eta = \frac{1}{2}\left(\frac{\partial^2 E}{\partial N^2}\right)_{\upsilon} \cong \frac{IP - EA}{2} \tag{2}$$

which measures the resistance to charge redistribution [10, 59]. The hardness, η, corresponds to the difference between the ionization and affinity energies. Chemical softness (σ) is defined as the inverse of η, $\sigma = 1/\eta$. When an electron acceptor (A) and donor (B) react, there is a net redistribution of electrons from B to A ($\mu_B > \mu_A$). As the product AB is formed, μ_A and μ_B equilibrate such that $\mu_A = \mu_B = \mu_{AB}$. Using this condition, Parr and Pearson [10] derived the amount of charge transfer term using Malone's ideas [61]:

$$\Delta N = \frac{1}{2}\frac{\mu_B - \mu_A}{\eta_B + \eta_A} \tag{3}$$

where μ_A and μ_B are the chemical potentials of the electrophilic and nucleophilic molecules, respectively. η_A and η_B are the respective hardnesses. Note that ΔN depends on the electrophilic system, and, therefore, there is not a unique nucleophilic scale. It will vary from one electrophile to another.

The global electrophilicity index was proposed by Parr, von Szentpaly and Liu [62]. It is associated with the power of an atom or a molecule to capture electrons. Considering a system as an electrophilic species inside a sea of free electrons and allowing for saturation of the electrophilic species with electrons, it follows that the stabilization energy of the system is equal to $\mu^2/2\eta$. Therefore, ω^+, as defined by Eq. 4, is a measure of the system's electrophilicity.

$$\omega^+ = \frac{\mu^2}{2\eta}. \tag{4}$$

2 Results and discussion

To facilitate the discussion, the geometrical parameters of the Hg(II) complexes are grouped into seven sets that are shown in the Supporting Information (Figs. S1–S7; B3LYP/cc-pVTZ//SDD(ECP) optimized structures): $[Hg(H_2O)_m]^{2+}$ (Fig. S1), $[Hg(Cl)_n(H_2O)_m]^{2-n}$ (Fig. S2), $[Hg(OH)_n(H_2O)_m]^{2-n}$ (Fig. S3), $[Hg(Cl)(OH)(H_2O)_m]^0$ (Fig. S4), $[Hg(S)_n(H_2O)_m]^{2-2n}$ (Fig. S5), $[Hg(SH)_n(H_2O)_m]^{2-n}$ (Fig. S6) and $[Hg(S)(SH)(H_2O)_m]^{1-}$ (Fig. S7). Selected structures are shown in Fig. 1 also. The molecular geometries of all participating species have been fully optimized at the B3LYP (G03) and PBE (ADF 2008) levels to obtain the equilibrium geometries that can be used for the subsequent calculations. The results and discussion is organized as follows: Geometries, harmonic vibrational frequencies, energetic analysis including hydration and reaction free energies and interaction energy, and, finally, the HSAB principle.

2.1 Geometries

2.1.1 Aqua complexes

Structures of water–Hg(II) clusters that include the first and second coordination spheres were optimized in the absence of a continuum solvent. Experimental [63] evidence suggests that the first solvation shell of the 5d Hg(II) metal ion is composed of six water molecules. Information on the second coordination shell is much scarcer than for the first hydration shell; however, we optimized the structures with a second hydration shell of seven to ten water molecules, Table 1.

The data in Table 1 show that a change from two to six water molecules increases the Hg–O bond length by almost 0.3 Å. From our calculations, we note that the number of the solvating ligands has a strong effect on the bond length and (possibly) bond strength. Until the point of saturation of the first solvation sphere at $m = 6$, we see monotonous increase in the average bond length. The short distance observed here for $m = 7$–10 with respect to 6 (for example,

Table 1 Comparison between the calculated values of the Hg(II)–oxygen distance in $[Hg(H_2O)_m]^{2+}$, $m = 2$–10, and the experimental measurements undertaken in the aqueous phase

m	Hg(II)–O/Å		
	1st Shell	2nd Shell	Other studies[b]
2	2.081		2.080
3	2.215		
4	2.288		2.270
5	2.351		
6	2.413		
7	2.396	4.091	
8	2.408	4.121	
9	2.406	4.142	
10	2.404	4.215	
Experimental[a]	2.34–2.41	4.10	

Average values

[a] Ref. [63]

[b] Ref. [108]

the Hg–O bond length is 2.413 Å and 2.396 Å for $[Hg(H_2O)_6]^{2+}$ and $[Hg(H_2O)_7]^{2+}$, respectively, Table 1) may merely be due to the second-shell waters that are experiencing attraction from the metal cation moving closer to it, thereby partly 'compressing' the first-shell waters. Moreover, the second-shell waters donate some electron density to the first-shell waters. As a consequence, this increases the attraction between the water in the first shell and Hg(II). Very similar effects of first- and second-shell waters on metal–ligand bond lengths are observed for the $[HgL_n]^q$ complexes also, see below.

2.1.2 Chloride complexes

The B3LYP-optimized Hg–Cl distances are 2.248 and 2.299 Å for the $[Hg(Cl)(H_2O)]^+$ and $[Hg(Cl)_2]^0$ complexes, respectively (Table 2, see also Fig. S2). This is somewhat close to the experimental range of 2.274–2.500 Å [64–68] and within 2.252–2.340 Å [69–74] range. In the remainder of this section, we will only discuss non-solvated complexes.

It appears that structures for other complexes included in the present study, particularly $[Hg(Cl)_3]^{1-}$ and $[Hg(Cl)_4]^{2-}$, have not been reported previously. The B3LYP-optimized HgCl bond lengths of the corresponding complexes are 2.473 and 2.619 Å, respectively, Fig. S2; Table 2.

2.1.3 Hydroxide complexes

The complexes $[Hg(OH)]^+$ and $[Hg(OH)_2]$ have not received much attention [75, 76]. Soldan et al. [75] studied mono-solvated Hg(II) and $[Hg(OH)]^+$ using B3LYP and several correlated ab initio methods. The Hg–OH bond length in the present study is 2.007 Å for $[Hg(OH)]^+$, Table 2. This is slightly longer than the MP2 result of 1.967 Å (Soldan et al.). Wang [76] reported that $[Hg(OH)_2]$ is stable and has a linear O–Hg–O angle. The Hg–OH bond length of the corresponding complex is 1.996 Å [109] at the B3LYP/6-311++G(3df, 3pd)//SDD level of theory. This bond length, in the present study, is 1.990 Å (Table 2 or Fig. S3), which agrees very well with the previous literature result that used high-level basis sets. This further confirms that our basis sets are close to convergence. The experimental Hg–OH bond length range of $[Hg(OH)_2]$ is

Table 2 B3LYP/cc-pVTZ//SDD (ECP) Hg–L_1 (Hg–L_2) equilibrium distances (Å) and harmonic vibrational frequencies (cm^{-1}; in square brackets, [HgL_1 (HgL_2)])

m	Calculated			
	R_{Hg-L}, Å [ν_{Hg-L}, cm^{1-}]			
	$[Hg(Cl)(H_2O)_m]^{1+}$	$[Hg(OH)(H_2O)_m]^{1+}$	$[Hg(SH)(H_2O)_m]^{1+}$	$[Hg(S)(H_2O)_m]^0$
0	2.286 [338.8]	2.007 [507.1]	2.362 [311.7]	2.295 [334.5]
1	2.248 (2.170) [360.3 (340.6)]	1.957 (2.153) [610.0 (386.8)]	2.312 (2.221) [385.1 (321.7)]	2.251 (2.409) [387.6 (224.2)]
5	2.279 [354.3]	1.989 [499.9]	2.324 [362.7]	2.277 [373.0]
6	2.278 [312.4]	1.982 [484.6]	2.327 [349.8]	2.310 [370.1]
7	2.324 [298.3]	2.076 [489.5]	2.360 [327.4]	
9	2.453 [285.2]	2.119 [451.0]	2.389 [287.1]	2.314 [359.0]
Expt[j]	2.301[a] [299.0][b]	1.967[c] [555.0][c]		

	$[Hg(Cl)_2(H_2O)_m]^0$	$[Hg(OH)_2(H_2O)_m]^0$	$[Hg(Cl)(OH)(H_2O)_m]^0$	$[Hg(SH)_2(H_2O)_m]^0$
0	2.299 [327.2, 381.5]	1.990 [544.0, 613.0][h]	2.295 (1.997) [354.3 (576.4)]	2.362 [312.2, 361.3]
4	2.380 [291.0, 328.6]	2.028 [508.3, 575.0]	2.343 (2.049) [325.3 (542.1)]	2.390 [296.2, 339.7]
6	2.446 [281.1, 290.9]	2.094 [442.4, 497.5]	2.336 (2.040) [332.3 (538.2)]	2.439 [271.8, 302.2]
Expt[j]	2.252–2.340[d] [355[e], 358[f], 313[g], 376[g]]	1.996[i] [551.0, 644.2][h]		

	$[Hg(S)_2(H_2O)_m]^{2-}$	$[Hg(S)(SH)(H_2O)_m]^{1-}$	$[Hg(Cl)_3(H_2O)_m]^{1-}$	$[Hg(Cl)_4(H_2O)_m]^{2-}$
0	2.372 [310.1, 343.8]	2.280 (2.461) [388.4, 266.8]	2.473 [260.9, 256.8, 246.5]	2.619 [210.0, 178.2, 178.5, 180.3]
2				2.607 [215.3, 182.0, 182.1, 193.0]
3			2.467 [263.1, 255.0, 258.3]	
4	2.364 [315.3, 348.0]	2.310 (2.421) [378.0, 290.5]		
6	2.360 [316.5, 352.1]	2.315 (2.420) [373.3, 291.0]	2.510 [265.3, 242.5, 224.2]	2.594 [221.3, 193.8, 194.0, 194.7]

[a] Ref [64]; [b] Ref [86]; [c] Calculated values using UMP2/ECP60MWB level of theory, see Ref [90]; [d] Ref. [e] Ref [69–74]; [f] Ref [87]; [g] Ref [88]; [h] Ref [90, 109]; [i] Ref [109]; [j] experimental values for $[Hg(L)]^{2-z}$ complexes, $m = 0$

2.00–2.10 Å [77, 78], slightly longer than for either of the optimized geometries.

2.1.4 Mixed chloride/hydroxide complexes

To our knowledge, there are no experimental or theoretical data on the structures of $[Hg(Cl)(OH)(H_2O)_m]^0$ complexes. However, Peterson et al. [34, 35, 39] applied the CCSD(T) method with different basis sets to study the structure and calculate the heat of formation of Hg(Cl)(O). [See Ref. [34] for a detailed discussion of Hg(Cl)(O)]. The optimized Hg–Cl and Hg–OH bond lengths of Hg(Cl)(OH) are 2.295 and 1.997 Å, respectively, Fig. S4 or Table 2. We can compare these with the bond lengths of HgCl, $Hg(Cl)_2$ and HgOH and $Hg(OH)_2$ (Table 2). From this comparison, we conclude that the presence of Cl^- or OH^- in the trans position will lengthen the Hg–Cl bond. The reverse effect is found for the Hg–OH bond length. This can be attributed to the donating ability of the ligands. The NBO analysis shows that the lone pair on the oxygen atom of the hydroxide group, Lp_O, is donating into the antibonding Hg–Cl orbital, σ^*_{HgCl}. This donation is stronger than the donation from the Cl^- lone pair, Lp_{Cl}, to σ^*_{HgOH}, resulting in the overall bond length effect.

2.1.5 HS^- and S^{2-} complexes

In aqueous media, Schwarzenbach and Widmer [79] suggested the (pH-dependent) species $[Hg(HS)_2]$, $[Hg(S)(HS)]^-$ and $[HgS_2]^{2-}$. In contrast, Barnes et al. [80] proposed four possible complexes, $[Hg(S)(H_2S)_2]$, $[Hg(HS)_3]^-$, $[Hg(S)(HS)_2]^{2-}$ and $[Hg(S)_2]^{2-}$, to model experimental results. On the other hand, Jay et al. [81] proposed that the complex, $Hg(S_x)_2^{2-}$, dominates the speciation of Hg(II) in the aqueous medium. Jay et al. [81] studied the effect of polysulfides on cinnabar [HgS(s)] solubility at lower S concentrations. They quantified a large increase in the solubility of cinnabar in the presence of elemental sulfur, particularly at high pH, while they reported that at lower sulfide concentrations and at high pH, the data are best fitted by considering also the formation of the species HgS_xOH^-. According to a different study by Barnes [82], $[Hg(HS)_2]$ is the dominant species at pH values less than 6, whereas $[Hg(S)(HS)]^-$ dominates between pH = 6 and 8, and $[Hg(S)_2]^{2-}$ above pH = 8; $[Hg(S)(HS)(OH)]^{2-}$ requires high pH values, which are outside the pH range of natural waters. Using ab initio methods, Tossell [42, 43] has calculated a number of structures for Hg–S complexes in which Hg is two-coordinate. The molecules $[Hg_2(S)(SH)_2]$, [Hg(S)], $[Hg(S)(H_2O)]$ and [Hg(SH)(OH)] were studied at various levels of theory [42, 43]. Lennie et al. [83] reported, from the comparison of calculated (2.399 Å) [42] and their experimental Hg–O distances (2.200 Å), that it is impossible to identify the coordinating oxygen as belonging to either H_2O or HO^-. In any case, for Hg–S complexes, Tossell [43] proposed $[Hg_3(S)_2(SH)_2]$ as being the best model to represent cinnabar since, at the HF level of theory, it best reproduces the Hg–S bond distance (2.390–2.410 Å) and S–Hg–S (179.0°) and Hg–S–Hg (96.0–104.0°) angles.

We have systematically explored the structures of Hg(II) complexes with sulfur, in the form of sulfide (S^{2-}) or bisulfide (HS^-). The studied complexes are: $[Hg(S)_n(H_2O)_m]^{2-2n}$, $[Hg(SH)_n(H_2O)_m]^{2-n}$ and $[Hg(S)(SH)(H_2O)_m]^{1-}$ for $n = 1$ and 2 and $m = 1, 5, 6, 7$ and 9 and 0, 4 and 6 (if $n = 2$), respectively. At the given B3LYP level of theory, we obtained optimized Hg–S distances of 2.295, 2.251, 2.372 and 2.280 Å for [Hg(S)], $[Hg(S)(H_2O)]$, $[Hg(S)_2]^{2-}$ and $[Hg(S)(SH)]^{1-}$, respectively, Table 2. Further, the optimized Hg(II)–bisulfide bond distances of $[Hg(SH)]^+$, $[Hg(SH)(H_2O)]^+$, $[Hg(SH)_2]$ and $[Hg(S)(SH)]^{1-}$ complexes are 2.362, 2.312, 2.362 and 2.461 Å, respectively, Table 2. The B3LYP calculations reproduce the experimental Hg–S distance to within 0.005 Å (for the Hg(S) complex, 2.30 Å) [83]. Likewise, the optimized structures of mono-hydrated cinnabar, $[Hg(S)(H_2O)]$, and Hg(II) coordinated with two sulfur ligands, $[Hg(S)_2]^{2-}$, are relatively close to the experimental Hg–S distances, 2.30 Å (EXAFS) and 2.35 Å (XRD), respectively [83]. The corresponding optimized bond lengths are 2.251 and 2.372 Å, respectively. The qualitative trends are as expected: The Hg–SH bond, $[Hg(SH)(H_2O)_m]^+$, $m = 0$ or 1, is longer than Hg–S, $[Hg(S)(H_2O)_{0\text{ or }1}]$, and the bond from Hg to –S in $[Hg(S)_2]^{2-}$ is slightly longer than that to –SH in $[Hg(SH)_2]$, Table 2. The presence of –S in the trans position of the $[Hg(S)(SH)]^{1-}$ and $[Hg(S)_2]^{2-}$ complexes increases the Hg–SH and Hg–S bond lengths by about 0.1 and 0.08 Å, respectively, while the presence of an aqua ligand in the trans position of $[Hg(SH)(H_2O)]^+$ and $[Hg(S)(H_2O)]^0$ complexes shortens the corresponding bonds by about 0.044 Å and 0.050 Å [40, 42], respectively. Finally, the presence of an –SH ligand in the trans position for the corresponding bonds shortens the Hg–S distance (by 0.015 Å) while having no effect on the Hg–SH bond length.

2.2 Frequencies of unsolvated species

B3LYP frequencies are known to be systematically higher than the experimental values. This would require multiplying the calculated frequencies by some scaling factor that is slightly smaller than 1. However, to the best of our knowledge, there is no tabulated scaling factor available for the B3LYP/cc-pVTZ//SDD (ECP) level of theory [84, 85]. Hence, we report the frequencies as calculated. The harmonic vibrational frequencies, calculated in the gas phase, are presented in Table 2.

The chloride complexes show a characteristic decrease in the Hg–Cl stretching frequencies with the lengthening in the corresponding bond. The calculated Hg–Cl stretching frequencies for Hg(Cl) and $Hg(Cl)_2$ are 338.8 and 327.2 (381.5) cm^{-1}, respectively, which are in reasonable agreement with experimental values (299.0 cm^{-1} for Hg(Cl) [86] and 313–365 cm^{-1} for $Hg(Cl)_2$ [87–90]). Both the experimental and calculated Hg–Cl stretching frequencies are correlated with the bond lengths.

The theoretical [90] and experimental [75] IR frequencies of the $[Hg(OH)]^+$ and $[Hg(OH)_2]$ complexes are 555.0 cm^{-1} (calculated at the UMP2/ECP60MWB level of theory) and 551.0 cm^{-1} (644.2 cm^{-1} asymmetric, as), respectively. Our calculated stretching frequencies of $[Hg(OH)]^+$ and $[Hg(OH)_2]$ are 507.1 cm^{-1} and 544.0 cm^{-1} [613.0 cm^{-1} (as)]. They are in agreement with the experimental values [75]. A decrease in the Hg–O stretching frequency is again directly correlated with an increase in the corresponding bond length, Table 2.

The concentrations of mercury sulfide species in aqueous solution are usually very small, so that their identification by spectroscopy is difficult. It might be possible to concentrate such species by using partitioning into organic solvents, and in this case, characterization by spectroscopic methods like IR/Raman, optical/UV absorption, EXAFS or XANES may be possible. Nevertheless, it is not currently possible to use these techniques to distinguish between the species $[Hg(SH)_2]$, $[Hg(S)(SH)]^{1-}$ and $[Hg(S)_2]^{2-}$. The calculated Hg–S and Hg–SH stretching frequencies might aid the spectroscopic characterization, Table 2. The trends are as expected: (1) The Hg–S frequencies increase when –SH is substituted by –S. (2) The Hg–(S)(S) stretching frequency is significantly lower than that of Hg–(S) and Hg–(S)(SH). (3) There is no significant difference in the stretching frequency between Hg–(SH) and Hg–(SH)(SH). (4) The stretching frequencies of Hg–(S)(SH) and Hg–(SH)(S) are higher than for both S^{2-} and SH^-, coordinated as mono-ligands to Hg(II), and lower than the corresponding frequencies when the ligands are coordinated as diligands to Hg(II).

2.3 Microsolvation effects

Cluster formation of a solute molecule with a few solvent molecules, such as H_2O, is known as microsolvation [91–95]. Experimental information on the structural details of the second hydration shell is generally scarcer than that for the first shell [63]. However, it is difficult, experimentally or theoretically, to judge whether the water molecules are in the first or in the second shell. Hence, we need to know whether there is a direct interaction (for first-shell waters) between the water and Hg(II) or not (2nd shell). In other words, we need some kind of criteria to establish whether the water molecules are in the 1st or 2nd shell. Here, we use three methodologies to solve this problem. They can be summarized as follows: (1) using the Hg–O distances and visual inspection in a graphical user interface, (2) NBO analysis (to determine which water molecules interact directly with Hg(II), and assign them to the 1st shell; then which water molecules interact with the 1st shell, but have no direct interaction with Hg(II)—those water molecules are assigned to the 2nd shell, and so on), and (3) the hydration free energy calculations. We will discuss the first two approaches in this section, while the third one will be discussed later in the energetic analysis section. Calculated Hg–O(H_2) distances are shown in Tables 1 and 3.

From visual inspection, bond lengths and NBO analysis, we find that the $[HgL_n(H_2O)_m]^q$ complexes can be classified into two categories: (1) One or more of the water molecules form a direct coordination bond with Hg(II). The rest of the water molecules constitute the second solvation shell, forming hydrogen bonds with the ligand, and act as electron donors. (2) None of the water molecules forms a coordination bond with Hg(II). Instead, they only form hydrogen bonds with the ligands. In this case, they act as electron acceptors [96–98].

In case 1, the Hg–L bond will lengthen as the number of coordination bonds around the Hg(II) increases. An example is provided by the series $[Hg(Cl)(H_2O)_5]^+$, $[Hg(Cl)(H_2O)_6]^+$, $[Hg(Cl)(H_2O)_7]^+$ and $[Hg(Cl)(H_2O)_9]^+$. The first complex has three water molecules coordinated to Hg(II), forming a distorted tetrahedral geometry. The second complex has two coordination bonds, forming a T-shaped structure, and the third and the last complexes have three and four coordination bonds forming a trigonal pyramid and square pyramid, respectively, see Fig. S2 (Supporting Information). The Hg–Cl bond lengths are 2.279, 2.278, 2.324 and 2.458 Å, respectively, directly reflecting the number of coordinated H_2O ligands.

In case 2, none of the water molecules forms a coordination bond with Hg(II). Instead, they only form hydrogen bonds, as acceptors, with the ligands. Thus, all the water molecules are considered as part of the second solvation shell. In this case, the corresponding ligand bond length will be shortened. This case is illustrated by $[Hg(Cl)_4(H_2O)_m]^2$ ($m = 0$, 2 and 6) and $[Hg(S)_2(H_2O)_m]^{2-}$ ($m = 0$, 4 and 6), Figs. S2 and 1; Table 2. The average Hg–Cl and Hg–S bond lengths show, in each series, decreasing Hg–L bond lengths. We note in passing that the aquo complexes, $[Hg(H_2O)_m]^{2+}$, fit into both categories.

The lengthening of the bonds in case 1 can be attributed to electron donation from the oxygen lone pair(s) of the coordinated water molecule(s), Lp_O, to the antibonding Hg–L orbital, σ^*_{Hg-L}. The shorter the Hg–OH_2 coordination bond distance(s), the stronger the electron donation and the longer the Hg–L bond length. Based solely on this

argument, $[Hg(Cl)(H_2O)_5]^+$ and $[Hg(Cl)(H_2O)_7]^+$ should have approximately the same Hg–Cl bond length. Instead, however, the Hg–Cl bond in the $[Hg(Cl)(H_2O)_7]^+$ complex is longer because of a hydrogen bond between one of the water molecules and the Cl^- ligand.

For case 1, the calculated total NBO charge on Hg(II), $Q_{Hg(II)}$, increases as the number of first and second hydration shell waters increases, in agreement with the preceding discussion, Table 3. The charge $Q_{Hg(II)}$ is inversely proportional to the distance between Hg(II) and the second-shell waters, $Hg–O_{II}$. This applies to cationic, neutral and mono-anionic species, Table 3.

The shortening of the corresponding bond lengths in case 2 can be explained through the decrease in charge density. For instance, in the above example, the average NBO charges of the Cl^- ligands are −0.66, −0.64 and −0.61 for $[Hg(Cl)_4]^{2-}$, $[Hg(Cl)_4(H_2O)_2]^{2-}$ and $[Hg(Cl)_4(H_2O)_6]^{2-}$, respectively. This decrease in the average charge of the Cl^- can be attributed to the hydrogen bond formation between the Cl^- ligands and the water molecules, which will decrease the negative charge density. As the negative charge decreases, the repulsion between the ligands decreases and the Hg–L bonds become shorter. Put differently, solvation through the second-coordination-sphere waters stabilizes the polar Hg–L bonds.

The $[Hg(S)(H_2O)_m]$ complexes are an exceptional case: As the number of water molecules increases, the Hg–S bond length, the $Hg–O_{II}$ distance and the charge, $Q_{Hg(II)}$, all increase. This can be attributed to the fact that the S^{2-} ligand is doubly negatively charged, and the water molecules form hydrogen bonds and act as electron acceptors, $Lp_S \rightarrow \sigma^*_{H–O}$ (proton donor [96–98]). This will decrease the negative charge on the S ligand. Hence, the attraction between the Hg(II) and S^{2-} decreases, and this is reflected in the bond length, Hg–S. As a result, the Hg–S bond is lengthened, which means less electron donation from S to Hg(II), and hence, the positive charge on Hg increases. This will also affect the $Hg–O_{II}$ distance.

For complexes with no water molecules coordinated with Hg(II), case 2, the Hg–L bond lengths decrease with an increasing number of water molecules. The $Hg–O_{II}$ distances and the $Q_{Hg(II)}$ charges decrease also. This is due to increased stability within the second-coordination-shell water cluster. Two examples are provided by the $Hg–O_{II}$ distances and the charges $Q_{Hg(II)}$ of $[Hg(Cl)_4(H_2O)_4]^{2-}$/$[Hg(Cl)_4(H_2O)_6]^{2-}$ and $[Hg(S)_2(H_2O)_4]^{2-}$/$[Hg(S)_6(H_2O)_4]^{2-}$, Table 3.

2.4 Energy analysis

In this section, we present the results of different types of energy analysis. These are the hydration free energy of hydrated clusters $[Hg(H_2O)_m]^{2+}$ (ΔG_{hyd}), the reaction free energy to form the complexes $[HgL_n(H_2O)_m]^q$ from $[Hg(H_2O)_6]^{2+}$ ($\Delta_r G$) and the interaction energy (E_{int}). The first one, ΔG_{hyd}, is used to determine the number of water molecules in the first shell. The second one, $\Delta_r G$, gives an indication regarding the basis set convergence. Furthermore, $\Delta_r G$ allows us to determine whether or not the addition of water molecules will increase the stability of Hg(II) complexes. Finally, E_{int} gives an indication of the effects of the ligand type and the number of water molecules on the electrons donation from the corresponding ligands to Hg(II).

2.4.1 $[Hg(H_2O)_m]^{2+}$ clusters: hydration energies

In this section, we consider the Gibbs free energy of hydration, ΔG_{hyd}, of Hg^{2+}. The hydration free energy, ΔG_{hyd}, provides an alternative means to determine how many water molecules are in the first hydration shell. ΔG_{hyd} is also an experimental thermodynamic parameter for the solvation of the metal ion.

The hydration free energy, ΔG_{hyd}, for a given hydrated cluster $Hg(II)–(H_2O)_m$ can be calculated as:

$$\Delta G_{hyd} = G_{Hg(II)-(H_2O)m} - (G_{Hg(II)} + mG_{H_2O}) \quad (5)$$

where $G_{Hg(II)–(H2O)m}$ refers to the free energy of the $[Hg(H_2O)_m]^{2+}$ cluster, $G_{Hg(II)}$ is the free energy of Hg(II) and $G_{(H2O)}$ is that of a single optimized H_2O molecule. The calculated (B3LYP) values of the free energies for Hg(II) and H_2O used to calculate the ΔG_{hyd} are −152.502116 and −76.456210 au, respectively. The basis set superposition error (BSSE) correction is done using the full counterpoise method [99]. The corrected values of the hydration energies are presented in Table S1.

The hydration free energy, ΔG_{hyd}, of the cluster, $[Hg(H_2O)_m]^{2+}$, increases with increasing the number of water molecules. The increase depends on the ion–solvent interaction, solvent–solvent H-bonding interactions and the orientation of the water molecules. Figure 2a shows the calculated ΔG_{hyd} as a function of the number of water molecules. The value of ΔG_{hyd} increases monotonously. From this figure, it is difficult to predict the coordination number of the Hg(II), which is the main idea of this section. So, to get a clearer picture, the incremental hydration free energy, $\Delta\Delta G_{hyd}$, is plotted in Fig. 2b.

The incremental hydration free energy has been calculated as:

$$\Delta\Delta G_{hyd} = G_{Hg(II)-(H_2O)m} - (G_{Hg(II)-(H_2O)m-1} + G_{H_2O}) \quad (6)$$

Figure 2b shows that the magnitude of the incremental hydration free energy decreases with increasing the number of water molecules around Hg(II) ion. Hartmann et al. [100] noticed similar effects for the microsolvation of Zn^{2+}. However, the charge from Hg(II) will diffuse to the

Table 3 The effect of the number of water molecules on the interaction energy, E_{int}, at the B3LYP(G03)/cc-pVTZ level

Complexes[a]	E^b_{int}	Q	6s	R_{Hg-OII}	Complexes[a]	E^b_{int}	Q	6s	R_{Hg-OII}	Complexes[a]	E^b_{int}	Q	6s	R_{Hg-OII}
$Hg(Cl)(H_2O)$	−352	1.219	0.862		$Hg(OH)(H_2O)$	−378	1.271	0.866		Hg(S)(H2O)	−625	0.786	1.201	
$Hg(Cl)(H_2O)_5$	−301	1.254	0.822	3.810	$Hg(OH)(H_2O)_5$	−354	1.313	0.822	3.690	$Hg(S)(H2O)_5$	−542	0.925	1.084	3.366
$Hg(Cl)(H_2O)_6$	−325	1.247	0.828	3.898	$Hg(OH)(H_2O)_6$	−378	1.292	0.837	3.737	$Hg(S)(H2O)_6$	−496	0.994	1.008	3.446
$Hg(Cl)(H_2O)_7$	−320	1.309	0.723	3.928	$Hg(OH)(H_2O)_7$	−332	1.412	0.624	3.750	$Hg(S)(H2O)_9$	−468	1.045	0.963	3.650
$Hg(Cl)(H_2O)_9$	−276	1.388	0.575	3.838	$Hg(OH)(H_2O)_9$	−293	1.418	0.577	3.713	$Hg(S)_2$	−608	0.836	1.117	
$HgCl_2$	−332	1.106	0.947		$Hg(OH)_2$	−360	1.179	0.976		$Hg(S)_2(H_2O)_4$	−534	0.886	1.108	4.233
$Hg(Cl)_2(H_2O)_4$	−254	1.240	0.761	3.990	$Hg(OH)_2(H_2O)_4$	−278	1.295	0.834	3.754	$Hg(S)_2(H_2O)_6$	−482	0.882	1.110	3.980
$Hg(Cl)_2(H_2O)_6$	−250	1.289	0.678	3.920	$Hg(OH)_2(H_2O)_6$	−268	1.352	0.704	3.704	$Hg(SH)(H_2O)$	−383	1.055	1.011	
$HgCl_3$	−258	1.190	0.772		Hg(Cl)(OH)	−92	1.147	0.954		$Hg(SH)(H_2O)_5$	−358	1.133	0.941	3.834
$Hg(Cl)_3(H_2O)_3$	−238	1.195	0.759	3.982	$Hg(Cl)(OH)(H_2O)_4$	−533	1.258	0.807	3.859	$Hg(SH)(H_2O)_6$	−362	1.136	0.938	3.956
$Hg(Cl)_3(H_2O)_6$	−235	1.233	0.707	3.919	$Hg(Cl)(OH)(H_2O)_6$	−517	1.238	0.825	3.694	$Hg(SH)(H_2O)_7$	−343	1.212	0.820	3.937
$HgCl_4$	−234	1.238	0.698		Hg(S)(SH)	−902	0.849	1.123		$Hg(SH)(H_2O)_9$	−304	1.243	0.757	3.942
$Hg(Cl)_4(H_2O)_2$	−224	1.250	0.685	4.209	$Hg(S)(SH)(H_2O)_4$	−868	0.895	1.101	4.126	$Hg(SH)_2$	−350	0.938	1.085	
$Hg(Cl)_4(H_2O)_6$	−202	1.237	0.688	4.162	$Hg(S)(SH)(H_2O)_6$	−859	0.905	1.094	3.956	$Hg(SH)_2(H_2O)_4$	−269	1.015	1.006	3.956
										$Hg(SH)_2(H_2O)_6$	−262	1.085	0.909	4.017

Total NBO charges, Q, and 6s AO occupancies on Hg(II) and the distance between Hg(II) and the second water shell

Interaction energies (Eq. 8) in kcal/mol

[a] Charges of complexes omitted. The actual complex charge is determined as the sum of Hg (2+) and ligand charges (Cl^-, HO^-, HS^- and S^{2-})

[b] E_{int} calculated between Hg(II) and ligands Cl^-, HO^-, HS^- and S^{2-}, Eq. 13

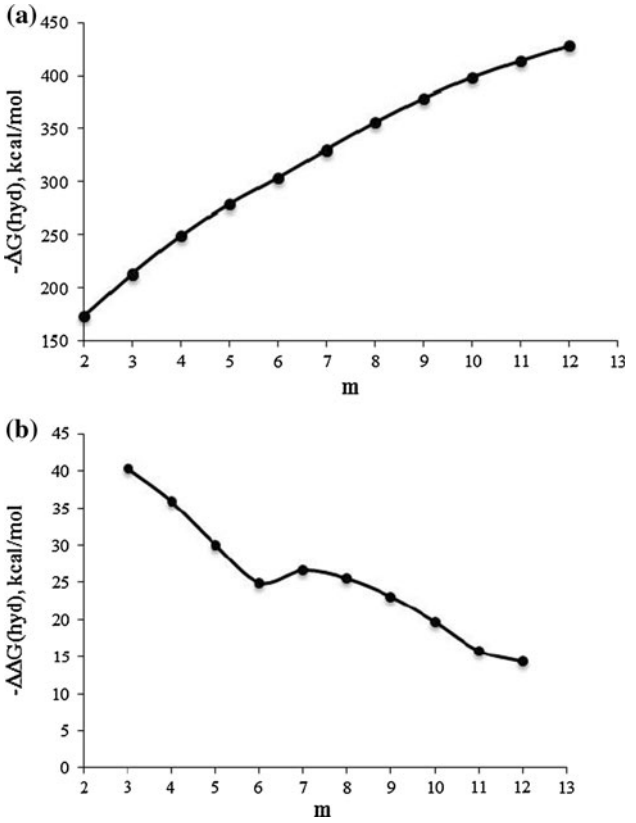

Fig. 2 Effect of water molecules number on the hydration and incremental free energies. **a** Hydration free energy, ΔG_{hyd} (Eq. 5), versus number of water molecules m in $[Hg(H_2O)_m]^{2+}$ clusters. **b** Incremental hydration free energy, $\Delta\Delta G_{hyd}$, versus number of water molecules, m, in $[Hg(H_2O)_m]^{2+}$ clusters

surrounding water molecules in the first coordination sphere. According to Fig. 2b, with increasing m, $\Delta\Delta G_{hyd}$ will decrease gradually up to the point where the first coordination sphere is filled ($m = 6$). Starting with $m = 7$, the second coordination sphere is being filled. Thus, it will be simply the effect of inter-water hydrogen bonding, in addition to the charge transfer and polarization effects that will occur from the Hg(II) ion to the 2nd shell through the 1st water shell and to the 3rd shell through the 1st and 2nd shells. Beginning with the second solvation shell, $m \geq 7$, the incoming water molecules simply interact through inter-solvent hydrogen bonding, as shown in Fig. 2b. However, if we compare the decrease in the $\Delta\Delta G_{hyd}$ values of $m = 8$ with respect to $m = 7$ and of $m = 9$ with respect to $m = 8$, we note a constant decrease (2 kcal/mol). It results from the H-bonding, and because of the particular symmetry for the 7th, 8th and 9th waters, we obtain the same value of decrease. This decrease is not constant anymore from $m = 10$ to 12 because of symmetry issues.

2.4.2 $[HgL_n]^q$ reaction free energies

In Table S2 are presented the B3LYP/cc-pVTZ//cc-pVTZ-PP (ECP) (G03) and PBE/TZ2P (ADF 2008) reaction free energies for the relevant complexes, starting from $[Hg(H_2O)_6]^{2+}$, reaction (7).

$$[Hg(H_2O)_6]^{2+} + xCl^- + yHO^- + zHS^- + z'S^{2-} \Downarrow \left[Hg(Cl)_x(OH)_y(SH)_z(S)_{z'}(H_2O)_m\right]^{2-x-y-z-2z'} + (6-m)H_2O \quad (7)$$

where $x + y + z + z' \leq 2$.

Reaction 7 represents the reaction of the hexaaqua-mercury complex with different ligands.

According to thermodynamic calculations [101], the divalent mercury in surface waters, Hg(II), is not present as the free ion Hg(II), but should be complexed in variable amounts to hydroxide ($[Hg(OH)]^+$, $[Hg(OH)_2]$) and chloride ions ($[HgCl]^+$, $[HgClOH]$, $[HgCl_2]$, $[HgCl_3]^-$, $[HgCl_4]^{2-}$) depending on the pH and the chloride concentration. It is also possible that, even in oxic surface waters, some or most of Hg(II) might be bound to sulfides (S^{2-} and HS^-), which have been measured at nanomolar concentrations in surface seawater [102]. The mercuric ion exhibits extremely high affinity for sulfide. This property controls the chemistry of mercury in anoxic waters and sediments. The speciation of dissolved Hg(II) in sulfidic waters is completely dominated by sulfide and bisulfide complexes ($[HgS_2H_2]$, $[HgS_2H]^-$, $[HgS]$ and $[HgS_2]^{2-}$). In this case, we can consider $x = y = 0$ (Eq. 7), and the complexes that can exist are $[Hg(S)_{z'}(H_2O)_m]^{2-2z}$, $[Hg(SH)_z(H_2O)_m]^{2-z}$, $[Hg(S)(SH)(H_2O)_m]$.

With reasonably converged basis sets, it is straightforward to calculate Δ_rG for reaction (7). Increasing the number of water molecules beyond $m = 4$ will not affect the hydration free energy, ΔG_{hyd} (Table S2; G03 calculations). We note that the reaction is exothermic in all cases. Increasing the value of m, that is, increasing the number of water molecules in the product, will convert Δ_rG into ΔG_{hyd}. ΔG_{hyd} can then be calculated for the following two reactions, (8) and (9), as shown in Eqs. 10 and 11:

$$[Hg(L)(H_2O)]^{+\text{or}\,0} + (m-1)H_2O \rightarrow [Hg(L)(H_2O)_m]^{+\text{or}\,0} \quad (8)$$

$$[Hg(L)_n]^{2-n\,\text{or}\,2-2n} + (m)H_2O \rightarrow \left[Hg(L)_n(H_2O)_m\right]^{2-n\,\text{or}\,2-2n} \quad (9)$$

$$\Delta_rG = \Delta G_{Hg(L)(H_2O)m} - \left[G_{(m-1)H_2O} + \Delta G_{Hg(L)(H_2O)}\right] \quad (10)$$

$$\Delta_rG = \Delta G_{Hg(L)n(H_2O)m} - \left[G_{(m)H_2O} + \Delta G_{Hg(L)n}\right] \quad (11)$$

Here, Eqs. 8 and 10 apply to the case of precisely one non-aqueous ligand L, whereas Eqs. 9 and 11 apply to the case of di or higher-coordinated Hg^{2+}, $n \geq 2$. Increasing the number of water molecules will not increase the

stabilization of the Hg(II)–L complexes. We can prove this by calculating the difference of the average hydration free energy, ΔG_{hyd}, between the large complexes ($m \geq 5$) within a given group, and the $\Delta_r G$ of the smallest complexes, within the same group, as shown in the following equation:

$$\Delta\Delta G_{hyd} = \left(\sum_m \Delta_r G_{m\gg 1}\right)/x - \Delta_r G^{(\text{smallest complex})} \quad (12)$$

where x represents the number of complexes. The results obtained from Eq. 12 are given in Table 4. With respect to the charge state, the complexes in this paper comprise mono-cationic with a single ligand, neutral with two ligands, neutral with a single ligand, anionic with two or three ligands, and dianionic with two or four ligands. The results in Table 4 indicate that the presence of the polar water molecules increases the stability of the charged Hg(II) complexes, while the stability decreases for the neutral ones due to the repulsion between water molecules. Thus, the data in Table 4 show that microsolvation will not guarantee an increase in the stability of the Hg(II) complexes. Instead, the charge of the complexes will control the stability of the complex in the presence of the water molecules. The presence of water molecules in a positively charged complex containing one ligand or a negatively charged complex containing two ligands will increase the stability of that complex. Two examples are $[Hg(OH)(H_2O)_m]^+$ and $[Hg(S)(SH)(H_2O)_m]^{1-}$ with $\Delta\Delta G_{hyd}$ values of −35.0 and −9.7 kcal/mol, respectively, Table 4. Generally speaking, the stability of the neutral complexes decreases with increasing the number of water molecules except for $[Hg(S)(H_2O)_m]^0$. This can be attributed to the large dipole moment of Hg(S) that allows for strong interactions with the polar water molecules. The stabilizing effect of the microsolvation can also be seen in the decreasing dipole moment of the overall solvated complex: The dipole moments of $[Hg(S)(H_2O)_m]$ are 8.94, 2.81, 2.13 and 2.57 D for $m = 1, 5, 6, 9$, respectively. The corresponding $\Delta\Delta G_{hyd}$ value is −10.6 kcal/mol, Table 4. On the other hand, the presence of the water molecules around $[Hg(L)(L')]^0$ complexes will affect the geometries and consequently the dipole moments. For example, the Cl–Hg–Cl angle in $[Hg(Cl)_2]^0$ angle is 180.0°. The corresponding angles are 161.4 and 149.6° for $[Hg(Cl)_2(H_2O)_4]^0$ and $[Hg(Cl)_2(H_2O)_6]^0$, respectively. Due to this, the overall dipole moments are 0.00, 1.11 and 1.66 D, respectively. The deviation from linearity increases with increasing the number of water molecules. This distortion is, according to the $\Delta\Delta G_{hyd}$ values in Table 4, unfavorable. The $\Delta\Delta G_{hyd}$ value is 5.2 kcal/mol, Table 4, amounting to destabilization.

Table 4 Free energy difference due to the presence of water molecules using cc-pVTZ//cc-pVTZ-PP (G03) basis set, Eq. 12

Reactions	$\Delta\Delta G^a_{hyd}$
$[Hg(Cl)(H_2O)]^+ + (m-1)H_2O = [Hg(Cl)(H_2O)_m]^+$	−38.49
$[Hg(OH)(H_2O)]^+ + (m-1)H_2O = [Hg(OH)(H_2O)_m]^+$	−35.00
$[Hg(SH)(H_2O)]^+ + (m-1)H_2O = [Hg(SH)(H_2O)_m]^+$	−29.19
$[Hg(Cl)_2]^0 + mH_2O = [Hg(Cl)_2(H_2O)_m]^0$	5.19
$[Hg(OH)_2]^0 + mH_2O = [Hg(OH)_2(H_2O)_m]^0$	2.36
$[Hg(SH)_2(H_2O)]^0 + mH_2O = [Hg(SH)_2(H_2O)_m]^0$	11.15
$[Hg(Cl)(OH)]^0 + mH_2O = [Hg(Cl)(OH)(H_2O)_m]^0$	2.97
$[Hg(S)(H_2O)]^0 + (m-1)H_2O = [Hg(S)(H_2O)_m]^0$	−10.55
$[Hg(Cl)_3]^{1-} + mH_2O = [Hg(Cl)_3(H_2O)_m]^{1-}$	−0.67
$[Hg(S)(SH)]^{1-} + mH_2O = [Hg(S)(SH)(H_2O)_m]^{1-}$	−9.70
$[Hg(Cl)_4]^{2-} + mH_2O = [Hg(Cl)_4(H_2O)_m]^{2-}$	−21.73
$[Hg(S)_2]^{2-} + mH_2O = [Hg(S)_2(H_2O)_m]^{2-}$	−44.47

[a] Free energy differences in kcal/mol

In the following sections, the effect of explicit solvent molecules on the interaction strength between Hg(II) and ligand L, the charge of Hg(II) complexes, and the charge transfer from ligand to Hg(II) will be discussed in more detail.

2.4.3 Interaction energies

Building on the ideas of Rulisek et al. [93], the interaction energy of the ligand L with the Hg(II) in the given coordinate geometry is defined as:

$$E_{int}(Hg,L) = \left\{\left[E\left(Hg(H_2O)_m(L)_n^{2-nz}\right) - E\left(Hg(H_2O)_m^{2+}\right)\right] - \left[E\left(Bq(H_2O)_m(L)_n\right) - E\left(Bq(H_2O)_m\right)\right]\right\}/n \quad (13)$$

(where $z = 0$, 1 or 2 is the absolute charge of the ligand L.) To directly compare the interaction energies of the Hg(II) cation in different modes of coordination, we use a computational approach (Eq. 13) that is closely related to, but slightly different from, the one proposed by Rulisek et al. First, we have optimized the molecular geometry and calculated the energy of the $[Hg(L)_n(H_2O)_m]^{2-nz}$ and $(Hg(H_2O)_m)^{2+}$ complexes. Subsequently, at the optimized geometry of the above complexes, the metal was substituted for a ghost atom Bq (i.e., only the basis functions are left at the metal center) and the energy of the $Bq(H_2O)_m(L)_n$ and $Bq(H_2O)_m$ systems computed. The total energy of a complex $[Hg(L)_n(H_2O)_m]^q$ can be viewed as composed of (1) the energies of the constituents, E(Hg), n * E(L), m * E(H_2O), and (2) the pair-wise interactions between these constituents. Within this type of model, the definition in Eq. 13 amounts to canceling all the terms except for the interaction between Hg and L, taken relative to an aquo complex. Thus, applying the term in curly brackets in Eq. 13 results in the interaction energy between

Hg and nL. Finally, dividing this by *n,* we will yield the desired interaction, Hg/L, Eq. 13. The water molecule has been chosen as appropriate reference ligand for two reasons: (1) It is possibly the simplest neutral ligand forming complexes with ionic character and (2) it models an explicit solvation model.

The metal–ligand distances and interaction energies of the different functional groups are strongly dependent on the number of water molecules around the central metal ion, Table 3. We shall discuss the interaction energy according to the ligand type and numbers and the total charge of the ligands surrounding the Hg(II).

Generally speaking, the order of E_{int} due to the ligand type in $[Hg(II)L]^{2-z}$ is $S^{2-} > HS^{-} > HO^{-} > Cl^{-} > H_2O$. The values of the corresponding interaction energies, E_{int}, are −732, −439, −438, −398 and −93 kcal/mol, respectively. The corresponding values for these ligands in the presence of one water molecule $[Hg(L)(H_2O)]^{2-z}$ show the same order, Table 3. Also, the interaction energy changes as a function of the trans-partner of the water molecule (Fig. 3). The decrease in $E_{int}(Hg–H_2O)$ in the presence of H_2O, HO^{-}, Cl^{-}, HS^{-} and S^{2-} ligands, Fig. 3, can be explained with the strength of the trans-effect of the ligand partner (ligand in the trans position with respect to H_2O, L–Hg–H_2O). The ligand partner transfers a certain part of its electron cloud onto the metal ion, thereby weakening the Hg–H_2O interaction.

Substituting the water molecule in $[Hg(L_1)(H_2O)]^{2-z}$ by a second ligand of the same type decreases the interaction energy between Hg(II) and the first ligand L_1 by about 20–30 kcal/mol. For example, the E_{int} between Hg(II) and Cl^{-} of $[Hg(Cl)(H_2O)]^{+}$ and $[Hg(Cl)_2]^{0}$ are −352 and −333 kcal/mol, respectively, and the E_{int} between Hg(II) and HS^{-} of $[Hg(SH)(H_2O)]^{+}$ and $[Hg(SH)_2]^{0}$ are −383 and −351 kcal/mol, respectively, Table 3. This decrease in the interaction energies can again be attributed to the trans-effect of the ligand partner.

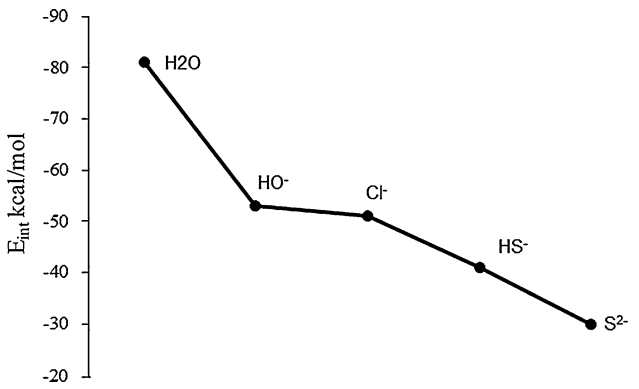

Fig. 3 Hg(II)–OH_2 interaction energy (Eq. 13) of $[L–Hg–OH_2]^{q}$ as a function of ligand type

We now turn to an analysis of the molecular orbitals of Hg(II) complexes. According to classical ligand field theory, the 6s atomic orbital (AO) becomes the LUMO of the Hg(II) fragment. The stability of the complex arises from bonding interactions of the vacant metal 6s orbital with the HOMO of the ligands fragment, which is composed of p_x, p_y or p_z orbitals. Since this is a two-electron/two-orbital interaction, the antibonding combination of these orbitals becomes the LUMO of the complex. Electrons are donated from the filled ligand orbital to the vacant metal orbital (σ donation). This decreases the total (positive) NBO charge of the Hg(II) atom by increasing the electron density in the Hg s orbital, Table 3. For instance, the interaction energy, the NBO charge of Hg(II) and the 6s occupancy of $[Hg(Cl)(H_2O)]^{+}$ are 352 kcal/mol, 1.219 and 0.86, respectively. The corresponding values of $[Hg(Cl)_2]^{0}$ are −333 kcal/mol, 1.106 and 0.95, respectively, Table 3. We note a similar trend also in $[Hg(OH)(H_2O)]^{+}$ and $[Hg(SH)(H_2O)]^{+}$ with respect to $[Hg(OH)_2]^{0}$ and $[Hg(SH)_2]^{0}$ complexes, Table 3. The character of the 5d orbitals of the Hg(II) atom becomes non-bonding. According to classical ligand field theory, these filled non-bonding orbitals provide a repulsive interaction with the entering ligand. The data in Table 3 indicate that the occupancy of the 6s orbital decreases linearly with E_{int}, while the opposite trend applies with respect to the total charge on Hg(II). This is exemplified by comparing the complex, before and after the addition of water molecules, within a given group $[Hg(L)_n(H_2O)_m]^{2-nz}$. Two examples are given by $[Hg(Cl)(H_2O)]^{+}$ and $[Hg(Cl)(H_2O)_{5,6,7\text{ and }9}]^{+}$ and $[Hg(SH)_2]^{0}$ and $[Hg(SH)_2(H_2O)_{4\text{ and }6}]^{0}$, Table 3.

From the interaction energy values between Hg(II) and water (E_{int}) and the occupancy of the 6s atomic orbital, the following sequence of trans ligands can be constructed as a measure of the strength of the trans-influence:

$$S^{2-} > HS^{-} > Cl^{-} \sim HO^{-} > H_2O$$

Figure 4 shows an inverse proportional relationship between the occupancy of the 6s AO and the total H_2O ligand charge. The total H_2O ligand charge reflects the amount of charge transferred by σ donation from the H_2O ligand to the 6s orbital. Based on this argument, one would expect that the above relationship should be proportional. The inverse proportional relationship between the two charges means that the σ-donating ability of the H_2O ligand is determined by the population of the 6s orbital. The higher the occupancy of the 6s AO, the lower the amount of charge that can be donated by the H_2O ligand to the Hg–OH_2 dative bond (and the longer the bond, Tables 3 and 5). Therefore, we can conclude that the trans-influence can be understood basically as a competition between the ligands in the trans positions for the ability to donate their electron density to the 6s AO of Hg.

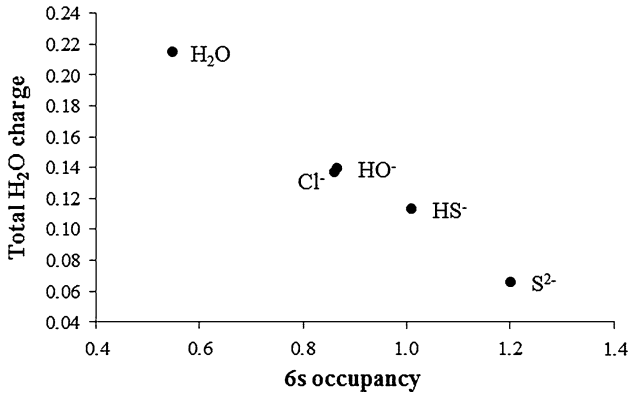

Fig. 4 Total NBO charge of the H_2O ligand versus AO occupancy of the Hg 6s orbital in $[Hg(L)(H_2O)]^q$ structures

Further evidence for this hypothesis is provided by NBO analysis of Hg(II) complexes in the presence of additional water molecules (microsolvation). In the presence of water molecules, the Hg(II) complexes deviate from linearity. For example, for $[Hg(Cl)(H_2O)]^+$ and $[Hg(Cl)(H_2O)_7]^+$, the angle $\theta_{H2OHgCl}$ is 178.7° and 163.5°, respectively. The nonlinear complexes show a decrease in 6s orbital occupancy and increase in total Hg(II) NBO charge compared with $[Hg(L)_n(H_2O)_m]^{2-nz}$. As the deviation from linearity increases, the positive charge on Hg(II) increases (Table 3). This is due to the decrease in the interaction between Hg(II) and ligand L, which will influence the 6s occupancy and the charge on Hg(II).

The water (H_2O) and the sulfide (S^{2-}) ligands are the weakest and the strongest nucleophilic ligands, respectively. The explanation of this order will be discussed further next.

2.5 HSAB principle

The Hg(II) ion is known as a soft Lewis acid [103]. According to the Pearson acid base concept, hard applies to species that are small, have high charge state and are weakly polarizable. Soft applies to species that are big, have low charge states and are strongly polarizable. Thus, Hg(II) is an electrophilic ion. The electrophilicity index (ω^+, Eq. 4) can be defined in terms of the hardness (η) and chemical potential (μ), Eq. 4 [62]. These two entities provide the global descriptors of the interaction between the Hg(II) ion and the studied ligands (Cl^-, HO^-, HS^- and S^{2-}) [10, 103, 104]. As mentioned previously, the electronic chemical potential, μ of Eq. 1, characterizes the tendency of electrons to escape from the equilibrium system, while η (Eq. 2) can be seen as a resistance to electron transfer. The electrophilicity establishes that the electron-donating or the electron-accepting ability may be quantified in terms of the chemical potential and chemical hardness, independent of the fractional amount of charge donated or accepted. However, charge acceptance stabilizes the system. So, larger values of ω^+ imply a larger capability to accept electron density, and vice versa for the donating process.

Although the environment (the solvent) plays an important role in most of the interactions (or reactions), very few studies have been undertaken to understand its effects on the interaction descriptors [105–107]. We have studied the effect of explicit solvent on the electrophilicity character of the $[Hg(H_2O)_m]^{2+}$ series, Fig. 5. As seen in this figure, the solvent has a strong effect on the global electrophilicity index of $[Hg(H_2O)_m]^{2+}$. The ω^+ value changes from 45.41 eV for the bare Hg(II) ion (the experimental electrophilicity of the bare Hg(II) is 45.24 eV) [103] to 33.94 eV for the system with one explicit water, $[Hg(H_2O)]^{2+}$. Similar variations, but in the opposite direction, can be found for the softness (σ), the inverse of the chemical hardness, upon explicit solvation for $[Hg(H_2O)_m]^{2+}$. The values for the calculated softness of Hg(II) and $[Hg(H_2O)]^{2+}$ are 0.061 eV^{-1} (the experimental value is 0.064 eV^{-1}) [103] and 0.076 eV^{-1}, respectively. The decrease in electrophilicity (ω^+) of $[Hg(H_2O)_m]^{2+}$ reflects a decrease in the chemical potential, or an increase in softness (σ), of Hg(II) in the presence of explicit water molecules. This will strongly affect the interactions between the metal and the ligands, Table 3; see also below.

The strength of the $[Hg(H_2O)_m]^{2+}$-to-ligand binding can be correlated with the charge transfer, ΔN of Eq. 3, Fig. 6a.

Table 5 B3LYP/cc-pVTZ (G03) and PBE/TZ2P (ADF 2008) geometries of $Hg(L_1)(H_2O)$ and $Hg(L_1)(L_{1\ or\ 2})$ structures (distances in Å)

$L_{1\ or\ 2}$	Softness[a]	$(H_2O)Hg–L_1$	$(L_1)Hg–H_2O$	$(L_1)Hg–L_1$	$(L_2)Hg–L_1$
Cl	−9.94	2.248 (2.232)	2.170 (2.162)	2.299 (2.281)	2.295 (2.277)
OH	−10.45	1.957 (1.954)	2.153 (2.144)	1.990 (1.990)	1.997 (1.997)
SH	−8.59	2.312 (2.299)	2.221 (2.218)	2.362 (2.354)	2.461 (2.278)
S	−6.29[b]	2.251 (2.234)	2.409 (2.390)	2.372 (2.369)	2.280 (2.451)
H_2O	−10.73		2.100 (2.082)		

PBE/TZ2P bond lengths are in parenthesis

[a] Ref [110].; [b] Calculated from a fit of the ligand softness versus the Hg(II) NBO charge fitted for the HS^-, OH^- and Cl^- ligands

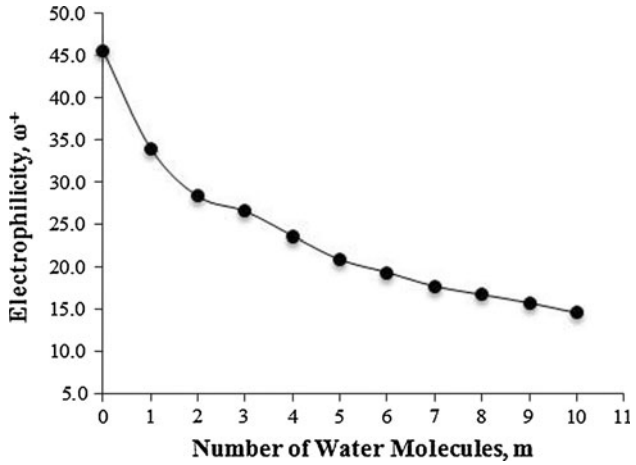

Fig. 5 Effect of explicit solvent on the global electrophilicity of $[Hg(H_2O)_m]^{2+}$, $m = 0$–10

A large positive value of ΔN is a harbinger of a strong interaction due to charge transfer from L to $[Hg(H_2O)_m]^{2+}$, while negative values of ΔN mean reverse charge transfer (back-donation). The charge transfer ΔN decreases as the number of water molecules increases. This is understandable from the fact that the global electrophilicity of $[Hg(H_2O)_m]^{2+}$ decreases with the number of water molecules (Fig. 5). The sulfide ligand gives the highest ligand-to-metal charge transfer, while the water ligand gives the lowest values and back-donation for $m \geq 2$, Fig. 6a. The presence of water molecules as ligands, forming coordination bonds with Hg(II), decreases the charge transfer ΔN from ligand L to Hg(II), consequently lengthening the Hg(II)–L bond length. The opposite reaction is one in which the water molecules act as electron acceptor, forming H-bonds with the ligand L. This results in charge transfer from ligand L to the Hg(II) ion, consequently shortening the Hg(II)–L bond length. We refer the readers to the microsolvation section (above). The charge transfer, ΔN, from H_2O, HO^-, Cl^- HS^- and S^{2-} to Hg(II) are 0.22, 0.59, 0.64, 0.76 and 0.84, respectively, Fig. 6a, while the corresponding values from S^{2-} to $Hg(H_2O)]^{2+}$, $[Hg(H_2O)_5]^{2+}$ and $[Hg(H_2O)_{10}]^{2+}$ are 0.68, 0.42 and 0.30, respectively, Fig. 6a.

As discussed above, the order of the interaction energies between Hg(II) and ligand L is: $S^{2-} > HS^- > HO^- > Cl^- > H_2O$ (Table 3; for comparison with respect to the experimental softness, see Table 5). This order is due to the strength of the nucleophilicity of the corresponding ligands. The respective nucleophilicity values are calculated as 6.15, 5.87, 5.38, 4.42 and 0.74 eV. The ΔN values ($m = 0$), due to bringing Hg(II) and L together, are 0.22, 0.64, 0.59, 0.76 and 0.84 for L = H_2O, Cl^-, HO^-, HS^- and S^{2-}, respectively, Fig. 6a.

The relative ΔN values of Cl^- and HO^- are in contradiction to the nucleophilicity strength and interaction

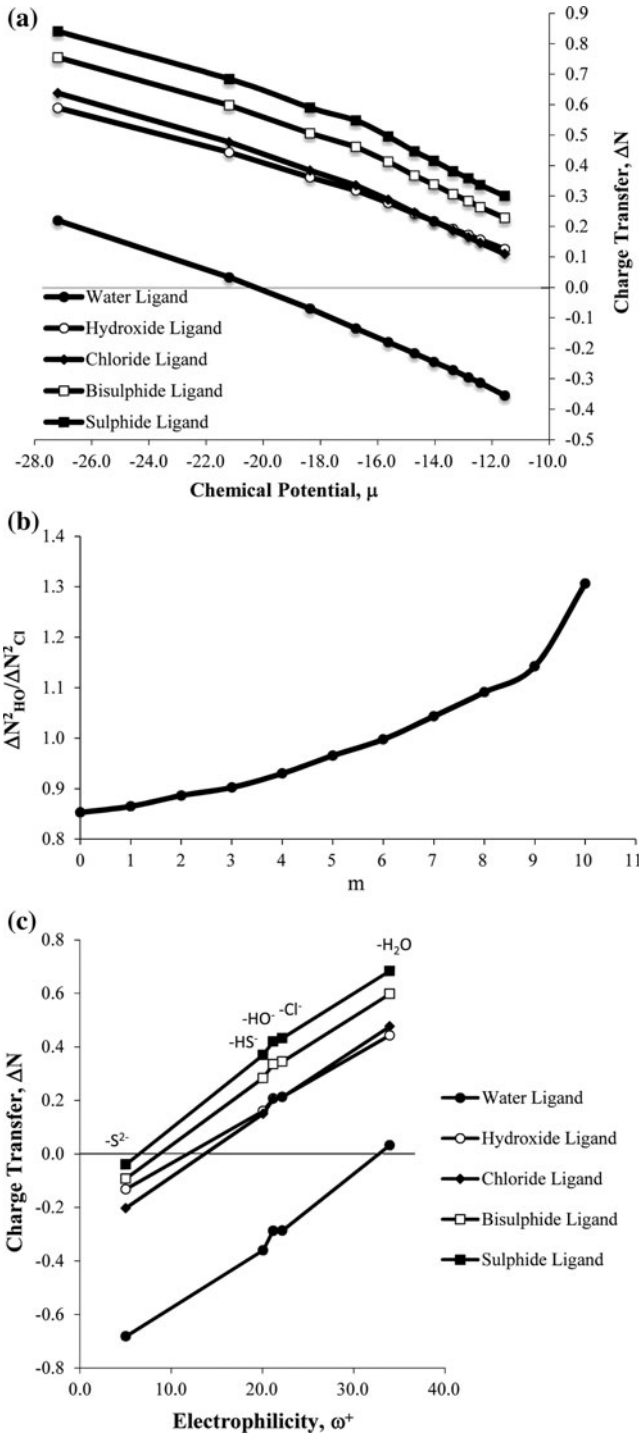

Fig. 6 **a** Correlation between the chemical potential, μ, of $[Hg(H_2O)_m]^{2+}$, $m = 0$–10, and the charge transfer, ΔN, due to different ligands. **b** Charge transfer ratio, $\Delta N^2_{HO}/\Delta N^2_{Cl}$, as a function of the number of water molecules. **c** Correlation between the electrophilicity of $[Hg(L_1)]^{2-q}$, where $L_1 = H_2O$, Cl^-, HO^-, HS^- and S^{2-}, and the charge transfer due to ligand L_2

energy values for $m = 0$–5. This can be attributed to the hardness control (Fig. 6a, b) on the charge transfer of the HO^- ligand where the nucleophilicity ratio $\omega^-_{Cl}/\omega^-_{OH}$ spans

the range 0.895–0.790 (ω^- is the nucleophilicity index). The hardness values of Cl^- and HO^- are 5.913 and 7.748 eV, respectively. We note also that the ΔN values of the corresponding ligands reverse their order at $m = 7$–10, Figure 6a, b. This is due to steric hindrance. The Cl^- ligand has a larger size than the HO^- ligand, which agrees with the nucleophilicity strength and the interaction energy values. In this case, the range of the nucleophilicity ratio, $\omega_{Cl}^-/\omega_{OH}^-$, is 0.731–0.584. At $m = 6$, the $\omega_{Cl}^-/\omega_{OH}^-$ ratio is 0.765, which is essentially equal to the hardness ratio between Cl^- and HO^-, 0.763.

The electrophilicity of Hg(II), 45.41 eV, decreases when the metal is coordinated with the above ligands. The global electrophilicity indexes of $[Hg(H_2O)]^{2+}$, $[Hg(Cl)]^+$, $[Hg(OH)]^+$, $[Hg(HS)]^+$ and $[Hg(S)]^0$ are 33.94, 22.17, 21.17, 20.06 and 5.06 eV, respectively, Fig. 6c. The reduction in the electrophilicity will decrease the charge transfer from ligand to Hg(II), and this is the reason for the decrease in the interaction energy values of $[Hg(L)_2]^q$, Table 3; Fig. 6c.

Finally, Fig. 7 shows that the charge transfer and the NBO charge on Hg(II) are strongly correlated. As mentioned previously, the values of the charge transfer, ΔN, can be used to represent the strength of the interaction (binding) between Hg(II) and ligand L. Also, the total NBO charge of Hg(II) represents the donating ability of ligand L to the 6s AO on Hg(II). The discussion of the dependence of the Hg(II) total NBO charge on the charge transfer, ΔN, can be summarized into three main points: First, increasing the positive value of the charge transfer will decrease the Hg(II) total NBO charge. Second, increasing the negative value of the charge transfer will increase the total NBO charge of Hg(II). Third, the charge transfer, ΔN, decreases due to a decrease in the electrophilicity of $[Hg(L)]^q$, which means that the Hg(II) has a less positive charge value. To illustrate the first point by an example, the S^{2-} case (the abbreviation means that we bring ligand S^{2-} and Hg(II) together) has a higher charge transfer, ΔN, than S^{2-}/H_2O (this means that we bring S^{2-} and $[Hg(H_2O)]^{2+}$ together) and consequently a lower Hg(II) total NBO charge. The corresponding values for S^{2-} and S^{2-}/H_2O are 0.840 (0.669) and 0.684 (0.786), respectively, Fig. 7. This means that the presence of a water molecule in the trans position will decrease the donating ability of the S^{2-} ligand. Moreover, the interaction strength between Hg(II) and S^{2-} is higher than between (H_2O)Hg(II) and S^{2-}. Another example for the first category is given by HS^-/H_2O 0.598 (1.055) and HO^-/Cl^- 0.213 (1.147). The second point concerns back-donation, Hg(II) to ligand charge transfer. Here, we have only four examples: S^{2-}/S^{2-}, HS^-/S^{2-}, $Cl^-/(Cl^-)_2$ and $Cl^-/(Cl^-)_3$, Fig. 7. The corresponding ΔN and Hg(II) total NBO charge values are −0.040 (0.836), −0.092 (0.849), −0.150 (1.190) and −0.389 (1.238), respectively, Fig. 7. Finally, the third point can be illustrated by the comparison of the corresponding values of HO^-/H_2O, 0.443 (1.271), with HO^-/HO^-, 0.207 (1.179).

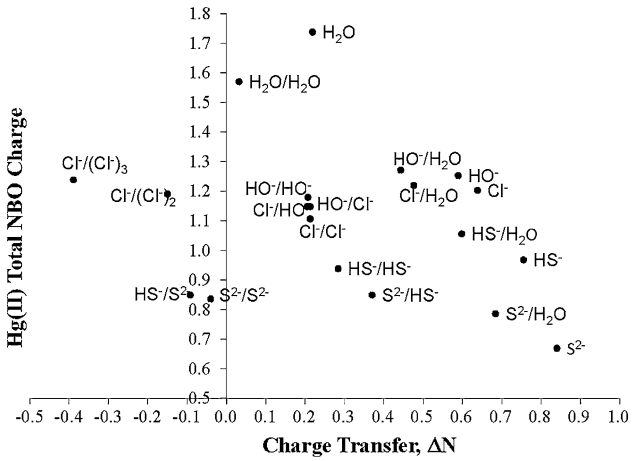

Fig. 7 Dependence of the total NBO charge of the Hg(II) atom in $[Hg(L_1)]^q$ and $[Hg(L_1)(L_2)]^q$ complexes on the charge transfer of ligand L_1. L_1 means we bring ligand L_1 and Hg(II) together. L_1/L_2 means we bring L_1 and $[Hg(L_2)]^{2-z}$ together

3 Conclusion

The present work reports various structural and thermodynamic parameters for the $[Hg(II)–(H_2O)_m]^{2+}$ clusters ($m = 2$–12) at the B3LYP (G03) and PBE (ADF 2008) levels of theory. The hydrated geometries where H_2O molecules are directly linked to the Hg(II) metal ion are less stable than the ones that have hydrogen bonding. It was found that Hg(II) is surrounded by six water molecules in the first hydration sphere for $m \geq 7$. The remaining waters form the second coordination sphere. For the hexaaquamercury cluster, the optimized Hg–OH_2 bond length is 2.413 Å, which is in excellent agreement with the X-ray diffraction data of 2.41 Å.

Overall, the calculations based on the computational procedure B3LYP/cc-pVTZ with SDD (ECP) and explicit solvation model produced a homogeneous set of data that connect very well to each other. The calculations indicate that the solvent has significant variable effect on the global electrophilicity (ω^+) of $[Hg(H_2O)_m]^{2+}$, the charge transfer (ΔN) and consequently the interaction strength between Hg(II) and ligand L. Moreover, it also affects the dipole moment, the atomic charge and the frontier orbitals inside each complex. NBO analysis indicates that the observed changes depend chiefly on the donation ability of the ligand. The charge transfer (ΔN), the Hg(II) total NBO charge and the interaction energies are strongly correlated.

Acknowledgments We acknowledge funding from the Natural Sciences and Engineering Council of Canada (NSERC).

References

1. Mason RP, Fitzgerald WF, Morel FMM (1994) Geochim Cosmochim Acta 58:3191
2. Schroeder WH, Munthe J (1998) Atmos Environ 32:809
3. Outridge PM, Macdonald RW, Wang F, Stern GA, Dastoor AP (2008) Environ Chem 5:89
4. Fitzgerald WF, Lamborg CH, Hammerschmidt CR (2007) Chem Rev 107:641
5. Henkel G, Krebs B (2004) Chem Rev 104:801
6. Schroeder WH, Anlauf KG, Barrie LA, Lu JY, Steffen A, Schneeberger DR, Berg T (1998) Nature 394:331
7. Lu JY, Schroeder WH, Barrie LA, Steffen A, Welch HE, Martin K, Lockhart L, Hunt RV, Boila G, Richter A (2001) Geophys Res Lett 28:3219
8. Steffen A, Schroeder W, Bottenheim J, Narayan J, Fuentes JD (2002) Atmos Environ 36:2653
9. Pearson RG (1963) J Am Chem Soc 85:3533
10. Parr RG, Pearson RG (1983) J Am Chem Soc 105:7512
11. Sigel H, McCormic DB (1970) Acc Chem Res 3:201
12. Martin RB (1987) J Chem Educ 64:402
13. Glusker JP (1991) Adv Protein Chem 42:1
14. Rulisek L, Vondrasek J (1998) J Inorg Biochem 71:115
15. Vedani A, Huhta DW (1990) J Am Chem Soc 112:4759
16. Comba P, Hambley TW, Strohle M (1995) Helv Chim Acta 78:2042
17. Comba P (1999) Coord Chem Rev 185–6:81
18. Ziegler T (1991) Chem Rev 91:651
19. Ziegler T (1995) Can J Chem-Rev Can Chim 73:743
20. Veillard A (1991) Chem Rev 91:743
21. Cory MG, Zerner MC (1991) Chem Rev 91:813
22. Deeth RJ (1995) Computational modeling of transition-metal centers. In: Coordination chemistry, structure and bonding, vol 82. Springer, Berlin, pp 1–42
23. Chermette H (1998) Coord Chem Rev 178:699
24. Niu SQ, Hall MB (2000) Chem Rev 100:353
25. Loew GH, Harris DL (2000) Chem Rev 100:407
26. Siegbahn PEM, Blomberg MRA (2000) Chem Rev 100:421
27. Frenking G, Fröhlich N (2000) Chem Rev 100:717
28. Hush NS, Reimers JR (2000) Chem Rev 100:775
29. Filatov M, Cremer D (2004) Chem Phys Chem 5:1547
30. Cremer D, Kraka E, Filatov M (2008) Chem Phys Chem 9:2510
31. Shepler BC, Balabanov NB, Peterson KAJ (2007) Chem Phys 127:164304
32. Shepler BC, Wright AD, Balabanov NB, Peterson KA (2007) J Phys Chem A 111:11342
33. Peterson KA, Shepler BC, Singleton JM (2007) Mol Phys 105:1139
34. Balabanov NB, Peterson KA (2004) J Chem Phys 120:6585
35. Shepler BC, Balabanov NB, Peterson KA (2005) J Phys Chem A 109:10363
36. Balabanov NB, Shepler BC, Peterson KA (2005) J Phys Chem A 109:8765
37. Balabanov NB, Peterson KA (2003) J Chem Phys 119:12271
38. Shepler BC, Peterson KA (2003) J Phys Chem A 107:1783
39. Balabanov NB, Peterson KA (2003) J Phys Chem A 107:7465
40. Tossell JA (2006) J Phys Chem A 110:2571
41. Tossell JA (2003) J Phys Chem A 107:7804
42. Tossell JA (2001) J Phys Chem A 105:935
43. Tossell JA (1999) Am Miner 84:877
44. Tossell JA (1998) J Phys Chem A 102:3587
45. Wiederhold JG, Cramer CJ, Daniel K, Infante I, Bourdon B, Kretzschmar R (2010) Environ Sci Technol 44:4191. doi: 10.1021/es100205t
46. Schauble EA (2007) Geochim Cosmochim Acta 71:2170
47. Frisch MJT, Trucks GW, Schlegel HB, Scuseria GE, Robb MA, Cheeseman JR, Montgomery Jr., JA, Vreven T, Kudin KN, Burant JC, Millam JM, Iyengar SS, Tomasi J, Barone V, Mennucci B, Cossi M, Scalmani G, Rega N, Petersson GA, Nakatsuji H, Hada M, Ehara M, Toyota K, Fukuda R, Hasegawa J, Ishida M, Nakajima T, Honda Y, Kitao O, Nakai H, Klene M, Li X, Knox JE, Hratchian HP, Cross JB, Bakken V, Adamo C, Jaramillo J, Gomperts R, Stratmann RE, Yazyev O, Austin AJ, Cammi R, Pomelli C, Ochterski JW, Ayala PY, Morokuma K, Voth GA, Salvador P, Dannenberg JJ, Zakrzewski VG, Dapprich S, Daniels AD, Strain MC, Farkas O, Malick DK, Rabuck AD, Raghavachari K, Foresman JB, Ortiz JV, Cui Q, Baboul AG, Clifford S, Cioslowski J, Stefanov BB, Liu G, Liashenko A, Piskorz P, Komaromi I, Martin RL, Fox DJ, Keith T, Al-Laham MA, Peng CY, Nanayakkara A, Challacombe M, Gill PMW, Johnson B, Chen W, Wong MW, Gonzalez C, Pople JA (2003) Gaussian 03, revision B.05; Gaussian, Inc.; Pittsburgh PA
48. Becke AD (1993) J Chem Phys 98:5648
49. Becke AD (1988) Phys Rev A 38:3098
50. Lee CT, Yang WT, Parr RG (1988) Phys Rev B 37:785
51. Vosko SH, Wilk L, Nusair M (1980) Can J Phys 58:1200
52. Fuentealba P, Preuss H, Stoll H, von Szentpaly L (1982) Chem Phys Lett 89:418
53. te Velde G, Bickelhaupt FM, Baerends EJ, Guerra CF, Van Gisbergen SJA, Snijders JG, Ziegler T (2001) J Comput Chem 22:931
54. van Lenthe E, Ehlers A, Baerends EJ (1999) J Chem Phys 110:8943
55. Ziegler T, Rauk A (1979) Inorg Chem 18:1755
56. Perdew JP (1986) Phys Rev B 33:8822
57. Baerends EJ, Ellis DE, Ros P (1973) Chem Phys 2:41
58. Reed AE, Curtiss LA, Weinhold F (1988) Chem Rev 88:899
59. Parr RG, Yang W (1989) Density functional theory of atoms and molecules. Oxford University Press, Oxford
60. Parr RG, Donnelly RA, Levy M, Palke WE (1978) J Chem Phys 68:3801
61. Malone JG (1933) J Chem Phys 1:197
62. Parr RG, von Szentpaly L, Liu SB (1999) J Am Chem Soc 121:1922
63. Ohtaki H, Radnai T (1993) Chem Rev 93:1157
64. Subramanian V, Seff K (1980) Acta Crystallogr Sect B-Struct Commun 36:2132
65. Liao MS, Zhang QE, Schwarz WHE (1995) Inorg Chem 34:5597
66. Schwerdtfeger P, Boyd PDW, Brienne S, McFeaters JS, Dolg M, Liao MS, Schwarz WHE (1993) Inorg Chim Acta 213:233
67. Kaupp M, von Schnering HG (1994) Inorg Chem 33:4179
68. Stromberg D, Stromberg A, Wahlgren U (1991) Water Air Soil Pollut 56:681
69. Braune HK, Knock SZ (1933) Phys Chem Abt B 23:163
70. Gregg AHH, Hampson GC, Jenkins GI, Jones PLF, Sutton LE (1937) Trans Faraday Soc 33:852
71. Akishin PA, Spiridonov VP (1957) Kristallografiya 2:475
72. Maxwell LR, Mosley VM (1940) Phys Rev 57:21
73. Deyanov PZ, Petrov KP, Ugarov VV, Shchedrin BM, Rambidi NG (1985) J Struct Chem 26:58
74. Kashiwabara K, Konaka S, Kimura M (1973) Bull Chem Soc Jpn 46:10
75. Soldan P, Lee EPF, Wright TG (2002) J Phys Chem A 106:8619
76. Wang X, Andrews L (2005) Inorg Chem 44:108
77. Göbbels D, Wickleder MS (2004) Acta crystallogr Sect EStruct Rep. Online 60:I40

78. Johansso G (1971) Acta Chem Scand 25:2799
79. Schwarzenbach G, Widmer M (1963) Helv Chim Acta 46:2613
80. Barnes HL, Romberger SN, Stembrok M (1967) Econ Geol 62:957
81. Jay JA, Morel FMM, Hemond HF (2000) Environ Sci Technol 34:2196
82. Barnes HL (1979) Solubilities of ore minerals, 2nd edn. Wiley, New York
83. Lennie AR, Charnock JM, Pattrick RAD (2003) Chem Geol 199:199
84. http://srdata.nist.gov/cccbdb/
85. Scott AP, Radom L (1996) J Phys Chem 100:16502
86. Uehara H, Konno T. Izaki Y, Horiai K, Nakagawa K, Johns JWC (1994) Can J Phys 72:1145
87. Braune HE, GZ (1932) Phys Chem Abt B 19:303
88. Clark RJHR, DM (1973) J Chem Soc Faraday Trans 2(69):1496
89. Sponer HT, Rev E (1941) Mod Phys 13:75
90. Aylett BJ (1973) Comprehensive inorganic chemistry. Pergamon Press, Elmsford
91. Jaque P, Marenich AV, Cramer CJ, Truhlar DG (2007) J Phys Chem C 111:5783
92. Li X, Tu Y, Tian H, Agren H (2010) J Chem Phys 132
93. Rulisek L, Havlas Z (2000) J Am Chem Soc 122:10428
94. Schreckenbach G, Shamov GA (2010) Acc Chem Res 43:19
95. Shamov GA, Schreckenbach G (2005) J Phys Chem A 109:10961. [Correction note: Shamov GA, Schreckenbach G (2006) J Phys Chem A 110:12072]
96. Keutsch FN, Cruzan JD, Saykally RJ (2003) Chem Rev 103:2533
97. Mas EM, Bukowski R, Szalewicz K (2003) J Chem Phys 118:4386
98. Xantheas SS (2000) Chem Phys 258:225
99. Boys SF, Bernardi F (1970) Mol Phys 19:553
100. Hartmann M, Clark T, van Eldik R (1997) J Am Chem Soc 119:7843
101. Stumm W, Morgan JJ (1996) Aquatic chemistry. Chemical equilibria and rates in natural waters. Wiley-Interscience, New York
102. Luther GW III, Tsamakis E (1989) Mar Chem 127:165
103. Pearson RG (1997) Chemical hardness. WILEY-VCH, Weinheim
104. Ayers PW, Parr RG (2010) J Am Chem Soc 2000:122
105. Chattaraj PK, Perez P, Zevallos J, Toro-Labbe A (2001) J Phys Chem A 105:4272
106. Perez P, Toro-Labbe A, Contreras R (2001) J Am Chem Soc 123:5527
107. Safi B, Choho K, Geerlings P (2001) J Phys Chem A 105:591
108. Cox H, Stace AJ (2004) J Am Chem Soc 126:3939
109. Solda PL, EPF, Wright TG (2002) J Phys Chem A 106:8619
110. Klopmann G (1968) J Am Chem Soc 90:223